

# Corrosion Resistances of Steel Pipe Coated with Two Types of Enamel by Two Coating Processes

Liang Fan, Fujian Tang, Genda Chen, Signo T. Reis, and Mike L. Koenigstein

(Submitted November 9, 2017; in revised form July 30, 2018; published online September 24, 2018)

The corrosion behaviors of uncoated, enamel-coated, and epoxy-coated steel samples were evaluated in 3.5 wt.% NaCl solution with open-circuit potential, electrochemical impedance spectroscopy and potentiodynamic polarization tests. Two types of enamel (powder and slurry) were coated on steel samples in electrostatic and wet spraying processes, respectively. Twelve 25 mm × 25 mm steel samples were cut from an API 5L X65 pipe of 323.850 mm in outer diameter and 9.525 mm in wall thickness. They were divided into four groups of three identical samples. Each group represents one of the four conditions: uncoated, powder enamel-coated, slurry enamel-coated and epoxy-coated. Scanning electron microscopy images revealed that the powder and slurry enamel coatings were approximately 180 and 235 μm thick, respectively. The powder enamel coating has fewer but larger isolated pores than the slurry enamel coating. Electrochemical tests consistently indicated that the powder and slurry enamel coatings provided slightly better and worse corrosion protection to the coated steel samples, respectively, than the epoxy coating. The charge transfer resistances of all the coated samples are approximately 10<sup>8</sup> times larger than that of the uncoated samples. All the coated samples were unlikely corroded within 2 h of immersion.

**Keywords** corrosion, electrochemical test, enamel coating, pipeline steel, scanning electron microscopy

## 1. Introduction

Internal corrosion can reduce the wall thickness and load capacity of metal pipes, leading to potential leakage or rupture of pipelines under internal and/or external pressures (Ref 1). Internal corrosion is affected by the chemical ingredients of transported commodities, crude oil or gas flow rate and operation temperature. In oil pipelines, the water transported along with crude oils can drop out of the crude oils and come in direct contact with the surface of pipes (Ref 2). When the water accumulates and remains on the pipe floor for an extended period of time, internal corrosion occurs. In gas pipelines, internal corrosion can take place when the internal surface is exposed to moisture and contaminants such as chlorides, CO<sub>2</sub> and sulfur compounds, that form electrolytes for electrochemical reactions (Ref 3).

To prevent internal corrosion, various measures can be taken during the design and operation of pipelines. For example, the quality of commodity can be controlled to minimize the chemical ingredients that cause or accelerate metal corrosion.

**Liang Fan** and **Genda Chen**, Department of Civil, Architectural, and Environmental Engineering, Missouri University of Science and Technology, Rolla, MO 65409-0030; **Fujian Tang**, State Key Laboratory of Coastal and Offshore Engineering, School of Civil Engineering, Dalian University of Technology, Dalian 116204 Liaoning, People's Republic of China; **Signo T. Reis**, Department of Materials Science and Engineering, Missouri University of Science and Technology, Rolla, MO 65409-0030; and **Mike L. Koenigstein**, Pro-Perma Engineered Coatings, Roesch Inc., Belleville, IL 62226. Contact e-mail: gchen@mst.edu.

Corrosion inhibitors can be added into transported liquids. Perhaps the most effective corrosion-protective approach is to apply internal coatings on the surface of metal pipes. In addition to corrosion prevention, internal coatings can reduce the surface roughness of metal pipes, which improves the efficiency of hydraulic flow and thus reduces energy consumption during the transport of liquids. Internal coatings can also improve the resistance of the pipe to erosion and cavitation and facilitate cleaning and water disposal after the hydrostatic testing of pipelines (Ref 4).

Internal pipeline linings can be divided into three main categories: concrete, rubber and plastics. Concrete lining can reduce the inner diameter of pipelines, and its roughness may consume high energy during operation. Rubber lining is not oil, flame and abrasion resistant, and it is susceptible to temperature change (Ref 5). Epoxy lining is vulnerable to cathodic disbondment with metal pipes.

Porcelain enamel, as an inorganic material, is chemically bonded to the substrate metal by fusing glass frits at a temperature of 750-850°C. It has been widely used in industry and domestic applications to protect metals or alloys from corrosion, including chemical reactors, heat exchangers, food-processing vessels and cookware. Even when locally breached, porcelain enamel remained chemically bonded to its substrate steel so that, with no presence of moisture underneath the enamel coating, corrosion was limited to the breached area and decelerated over time as oxygen was reduced (Ref 6). In addition to excellent chemical stability and good corrosion resistance, porcelain enamel has excellent resistances to abrasion, heat, and mechanical and thermal shocks particularly in extreme wear and erosion applications (Ref 7).

Fluorine-free enamel for pipeline internal lining was developed to improve chemical resistance and impact strength (Ref 8). By comparing the characteristics of known materials, silicate enamel coating was found most effective and promising in extending the service life of steel pipes; it can increase the pipeline operating temperature to 400°C (Ref 9). Non-nickel

low-melting one-coat enamel was also developed for environment-friendly applications in pipeline lining (Ref 10). By analyzing the technical and operational properties of a series of enamel coatings for pipeline protection, the newly synthesized enamel coatings exhibited higher adhesions and chemical resistances to corrosive media (Ref 11). However, the deposition of the enamel coatings on the inner surface of pipes was all carried out with a wet (slip) slurry procedure and no electrostatic process has been used before. An electrostatic spray process uses lighter enamel powder (instead of slurry), which is easier to remain in the crown area of pipe wall under gravity, and shorter in coating time without the need for drying. In addition, no electrochemical tests were conducted to characterize the corrosion resistance of electrostatically sprayed enamel coating on steel substrates.

This study aims to select and characterize new enamel coatings so that their corrosion resistances are competitive to the widely used epoxy coating in specified applications. Two types of enamel coatings are applied on steel samples in electrostatic and wet spraying processes. Their corrosion behaviors are systematically investigated and compared with that of epoxy-coated samples in 3.5 wt.% NaCl solution with open-circuit potential, electrochemical impedance spectroscopy and potentiodynamic polarization tests. Their microstructures are examined with scanning electron microscopy to help interpret electrochemical test results.

## 2. Materials and Methods

### 2.1 Sample Preparation

An API 5L X65 steel pipe (MRC Global Inc.) was selected as a substrate material due to its wide applications in pipeline industry. The pipe is 323.850 mm in outer diameter and 9.525 mm in wall thickness with a chemical composition (wt. %): C 0.17, Mn 1.15, P 0.07, S 0.02, Si 0.26, Cu 0.1, Ni 0.04, Cr 0.07, Mo 0.07, Al 0.024, V 0.02 and Fe balance. Prior to coating, a full-size pipe was cut into 12 coupon samples (25 mm × 50 mm). The samples were then annealed in a muffle furnace at 850°C for 2 h for decarburization pretreatment. Once taken out of the furnace, all the samples were steel blasted for 1 min and cleansed with a commercially available cleansing solvent.

Steel coupon samples were coated with enamel powder (PEMCO Product) in a dry process and with enamel slurry (Tomatec Product) in a wet process. In the dry process, the enamel powder was electrostatically sprayed on the surface of each sample, fired at 843°C for 10 min and finally cooled down to room temperature. In the wet process, the enamel slurry was prepared by milling a mixture of glass frits, clay and certain electrolytes, and adding water until the mixture remained in a stable suspension state. The water, glass frits, and clay were mixed in a proportion of 1.00: 2.40: 0.17 by weight. The enamel slurry was sprayed directly on the surface of each

sample, heated at 150°C for 10 min to drive off moisture, fired at 815°C for 10 min and finally cooled down to room temperature. The chemical compound of powder and slurry enamel coatings, determined from x-ray fluorescence (XRF) tests, is presented in Table 1. For repeatability, three samples were prepared with each coating conditions. They are designated as P-1, P-2 and P-3 for enamel powder, and S-1, S-2 and S-3 for enamel slurry.

For comparison, three uncoated (UN-1, UN-2 and UN-3) and three epoxy-coated (EP-1, EP-2, and EP-3) steel samples were also prepared and tested. The 3 M Scotchkote 323 two-part epoxy, which is designed to help protect steel from corrosion, was brushed to the surface of each sample at room temperature and dried in air for 3 days prior to electrochemical tests. The applied coating has a coating thickness of 400 μm, a surface roughness of 0.92 μm and a pull-off strength of 10 MPa.

### 2.2 Coating Characterization

Cross sections of enamel-coated samples were prepared before and after corrosion tests to examine the enamel microstructure and investigate the elemental analysis of the coatings with scanning electron microscopy (SEM, Hitachi S-4700, Tokyo) coupled with an energy-dispersive x-ray spectroscopy (EDS). Each enamel-coated sample was cold-mounted in epoxy resin (EpoxyMount, Allied High Tech Products, Inc.), and cut into a 10-mm thick cross section using a diamond saw. The 10-mm thick slices were then abraded with silicon carbide papers with grits of 80, 180, 320, 600, 800 and 1200. After abrading, all samples were rinsed with deionized water and dried at room temperature prior to SEM imaging. ImageJ was used to calculate the porosity of each coating. The porosity is defined to be the ratio between the bubble area and the entire area of a SEM image.

### 2.3 Corrosion Tests

To prepare for electrochemical tests, a copper wire was electrically connected to each sample. All sides of a sample except the enamel- or epoxy-coated surface were covered with Marine epoxy (LOCTITE) to force any electrochemical reaction through the coating surface. The exposed enamel or epoxy coating area was 30 mm by 20 mm in size as shown in Fig. 1.

For corrosion tests, all samples were immersed in 3.5 wt.% NaCl solution (Fisher Scientific, Inc.). Steel samples were tested at room temperature with a typical three-electrode setup, including a 25.4 mm × 25.4 mm × 0.254 mm platinum sheet as the counter electrode, a saturated calomel electrode (SCE) as the reference electrode and the steel coupon as a working electrode. All three electrodes were connected to an Interface1000E Potentiostat (Gamry Instrument) for data acquisition. The open-circuit potentials (OCPs) of the samples were recorded for 1 h immediately after the samples had been immersed in the solution. Electrochemical impedance spectroscopy (EIS) data were sampled at ten points per decade

**Table 1** Chemical compound of borosilicate glasses (wt.%)

Elements	SiO <sub>2</sub>	B <sub>2</sub> O <sub>3</sub>	Na <sub>2</sub> O	CaO	MnO <sub>2</sub>	Al <sub>2</sub> O <sub>3</sub>	TiO <sub>2</sub>	K <sub>2</sub> O	Fe <sub>2</sub> O <sub>3</sub>	MgO	BaO	Others
Enamel slurry (S series)	60.3	12.84	7.20	2.37	5.37	4.49	0.14	2.12	3.48	0.17	1.47	0.05
Enamel powder (P series)	57.5	16.95	9.60	3.31	4.70	1.02	1.41	3.63	1.49	0.21	0.04	0.14

around the OCP ( $E_{ocp}$ ) with a sinusoidal wave of 10 mV in amplitude and frequency ranging from 100 kHz to 5 mHz. After the EIS tests, potentiodynamic polarization (PP) tests were conducted from  $E_{ocp} - 300$  mV to  $E_{ocp} + 1500$  mV with a scanning rate of 5.0 mV/s.

### 3. Results and Discussion

#### 3.1 Coating Microstructure

Cross-sectional SEM images and representative EDS analyses of enamel-coated steel samples are presented in Fig. 2. EDS analyses were performed on the coating sample taken within the small white square in the respective SEM images. Powder enamel coating (P series) of approximately 180  $\mu\text{m}$  in thickness as shown in Fig. 2a-1 has an amorphous structure

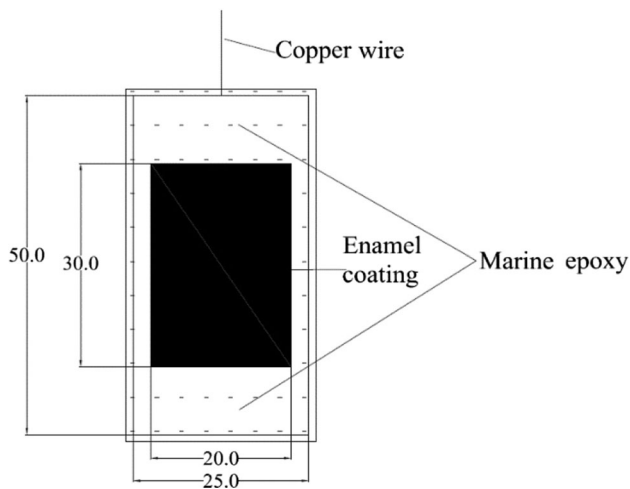


Fig. 1 Test sample dimension (unit: mm)

with a few isolated air bubbles corresponding to a porosity of 3.51%. The largest air bubble is 41  $\mu\text{m}$  in diameter. The magnified interface layer as shown in Fig. 2a-2 shows the extensive formation of an island-like structure in the enamel coating, reinforcing interfacial bond (Ref 12). EDS analysis as shown in Fig. 2a-3 indicates that the principal components in the coating include silicon (Si), sodium (Na), manganese (Mn), potassium (K), calcium (Ca), iron (Fe), titanium (Ti) and aluminum (Al); boron, a major component of the glass frit, could not be detected by the EDS system used due to its light weight.

The slurry enamel coating (S series) as shown in Fig. 2b-1 is approximately 235  $\mu\text{m}$  thick and has a porosity of 6.57%. It has more but smaller air bubbles than the powder enamel coating. Figure 2b-2 also shows anchor points growing into the coating, indicating strong chemical bond at the enamel-steel interface. EDS analysis in Fig. 2b-3 indicates that silicon (Si), sodium (Na), manganese (Mn), aluminum (Al), iron (Fe), calcium (Ca), potassium (K) and barium (Ba) are the detected principal components; EDS analysis could not detect boron.

The air bubbles in the coating were formed in the enameling process by entrapped gases such as  $\text{H}_2$ , CO and  $\text{CO}_2$ . During the firing process, the dissolved oxygen reacted with carbons in the steel, releasing gaseous CO/ $\text{CO}_2$ . The atomic hydrogen diffused into the steel to form hydrogen gas ( $\text{H}_2$ ). In the cooling process, the gases  $\text{H}_2$ , CO and  $\text{CO}_2$  were no longer able to escape since the gases were entrapped in the solidified enamel (Ref 12, 13).

#### 3.2 OCP Tests

The OCP represents the potential between the working electrode and the reference electrode when no external potential is applied to the test system. Figure 3 presents the OCPs of uncoated, enamel- and epoxy-coated steel samples after 1 h of immersion. The variation in OCP among the three identical uncoated samples is much smaller than that of the enamel- and epoxy-coated samples. The average OCP of three uncoated

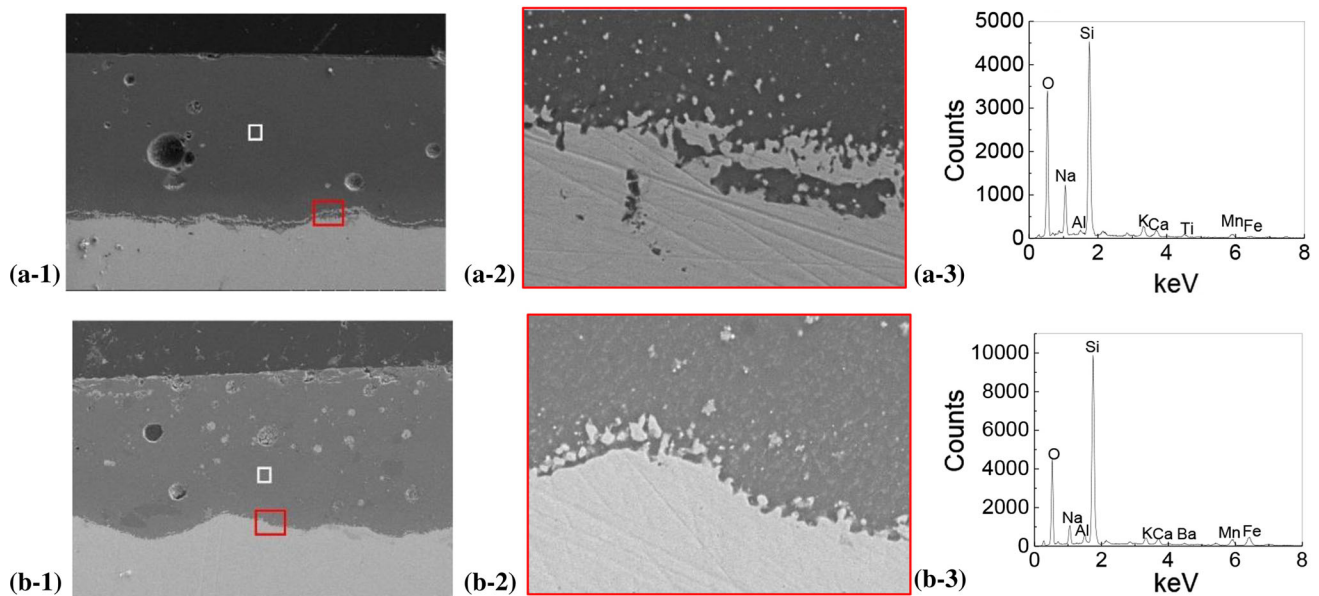


Fig. 2 Cross-sectional SEM images and EDS analysis of (a-1, a-2, a-3) powder enamel-coated sample and (b-1, b-2, b-3) slurry enamel-coated sample before corrosion tests with different magnifications: (a-1) 250 $\times$ , (a-2) 2500 $\times$ , (b-1) 250 $\times$  and (b-2) 2500 $\times$

steel samples shows a gradually decreasing trend from the beginning of  $-0.39$  V to the end of  $-0.48$  V. The average OCPs of the powder and slurry enamel-coated samples increase rapidly in the first 500 s due to the capacitive charging of enamel coating and then slowly approach to an asymptotical value of 0.88 and 0.4 V, respectively. The OCP changing trends of three epoxy-coated samples are inconsistent. However, the OCP of each sample after 1 h of immersion remains positive with an average value of 0.2 V. Compared with the uncoated steel samples, the higher positive OCP values of enamel- and epoxy-coated samples imply a superior barrier effect to the penetration of electrolyte through the open pores or localized defects. Thus, the coated samples can prevent the electrolyte from being in contact with the substrate steel.

### 3.3 EIS Tests

The electrochemical impedances of uncoated, enamel- and epoxy-coated samples are presented in the format of Bode plots in Fig. 4. In the Bode diagrams, the impedances and phase angles among the three identical samples with each coating are quite consistent. The impedance diagrams of enamel- and epoxy-coated samples show a  $45^\circ$  slope in a log-log scale while those of the uncoated samples start with a slope of larger than  $45^\circ$  at low frequency and gradually decrease to  $0^\circ$  at high frequency. The impedances of all the enamel- and epoxy-coated samples at a frequency of 0.005 Hz are approximately  $4 \times 10^{10} \Omega \text{ cm}^2$ . Although relatively low due to potential coating defects, the impedances are  $10^9$  times higher than those of the uncoated samples. In addition, the phase angles of the enamel- and epoxy-coated samples approach to  $90^\circ$  at high frequency while those of the uncoated samples are close to  $0^\circ$ . The phase angle diagrams confirm that both the enamel and

epoxy coatings provide high resistances to the penetration of electrolyte and thus satisfactory corrosion protection (Ref 14).

Two electrical equivalent circuit (EEC) models were chosen to fit the experimental data (Ref 15, 16) as illustrated in Fig. 5. Models (a) and (b) were used to simulate the uncoated and coated samples, respectively. In the two models,  $R_s$  represents the solution resistance,  $R_c$  and  $R_{ct}$  represent the pore resistance of coating and the charge transfer resistance at the steel-electrolyte interface, respectively, and  $CPE_c$  and  $CPE_{dl}$  represent the contribution of coating capacitance and double-layer capacitance to the total impedance, respectively.  $CPE_c$  and  $CPE_{dl}$  were used to replace pure capacitances because of the non-homogeneity in coating thickness and roughness (Ref 17, 18) and a distribution of electrochemical reactivity on the substrate steel, respectively (Ref 19). The impedance of a CPE is represented by:

$$Z_{CPE} = Y^{-1}(j\omega)^{-n} \quad (\text{Eq 1})$$

where  $Y$  is a CPE constant,  $\omega$  is the angular frequency and  $n$  ( $0 \leq n \leq 1$ ) is an index that represents the deviation from a pure capacitor (Ref 20). The effective capacitance can be obtained by (Ref 21, 22):

$$C = Y^{1/n}R^{(1-n)/n} \quad (\text{Eq 2})$$

where parameters  $R_c$ ,  $Y_c$  and  $n_c$  are used to calculate the effective capacitance of enamel coatings  $C_c$ , and  $R_{ct}$ ,  $Y_{dl}$  and  $n_{dl}$  are used to calculate the effective capacitance of double layer  $C_{dl}$ .

For the uncoated samples, there is only one time constant corresponding to the electrochemical reaction at the steel-electrolyte interface. For the enamel- and epoxy-coated sam-

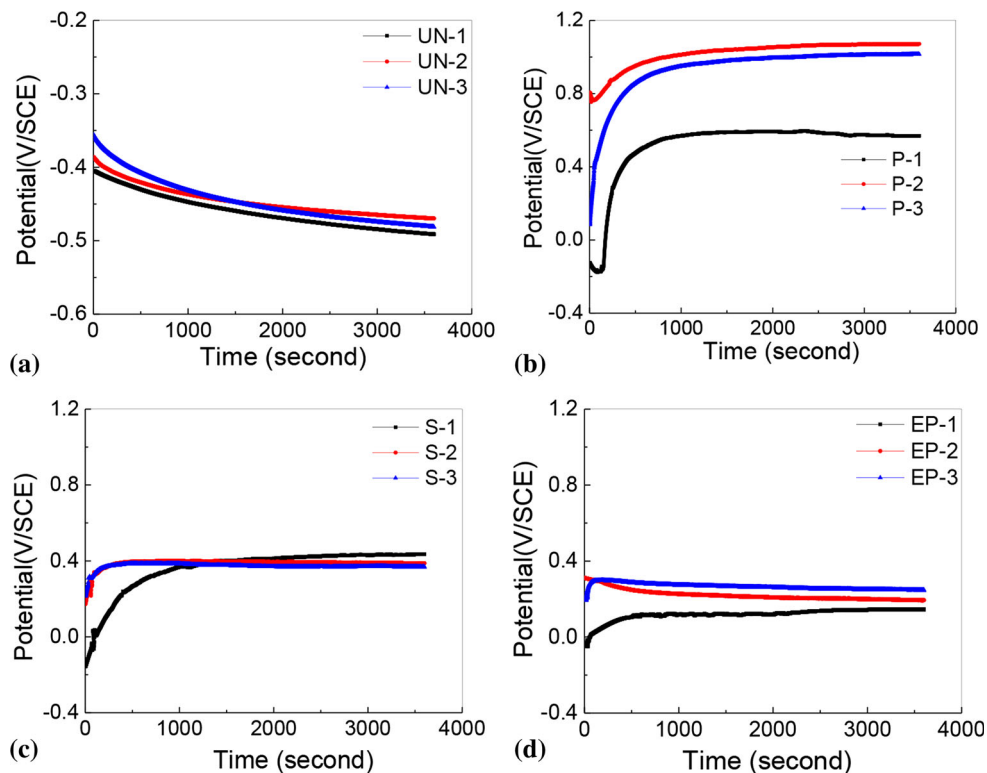


**Fig. 3** The OCPs of various samples in 3.5 wt.% NaCl solution: (a) uncoated, (b) powder enamel-coated, (c) slurry enamel-coated and (d) epoxy-coated steel samples

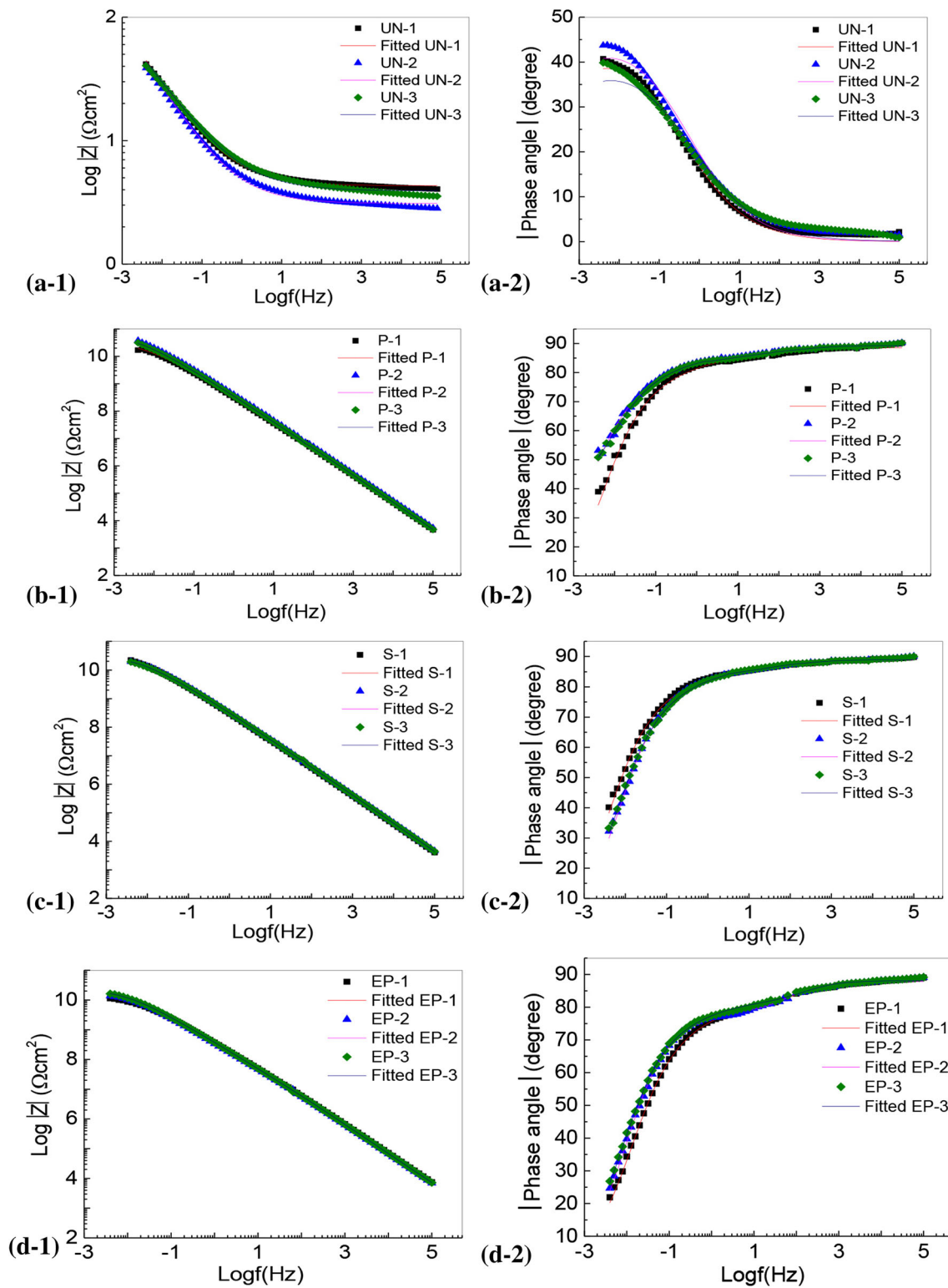


**Fig. 4** EIS diagrams (1 and 2: Bode plot) for: (a) uncoated, (b) powder enamel-coated, (c) slurry enamel-coated and (d) epoxy-coated steel samples

ples, there are indeed two time constants, which correspond to the electrochemical reaction at the steel–electrolyte interface and the dielectric properties of coatings (Ref 20, 23). In the Bode plots, the two time constants are not easily identifiable since they are overlapped (Ref 24).

ZSimpWin was used to determine the parameters of two EEC models based on the EIS data recorded. The Chi-squared values were in the order of  $10^{-4}$  to  $10^{-3}$  for all the samples, indicating a satisfactory fitting of the two proposed EEC models. The parameters obtained from curve fitting are listed in Table 2.

In general, the pore resistance represents the ability of coating to resist the penetration of electrolyte solution while the coating capacitance indicates the ease of electrolyte diffusion into the coating. Both parameters are closely related to the dielectric property and microstructure of the coating [25, 26]. As shown in Table 2, the pore resistances of all the enamel- and epoxy-coated samples are between  $10^7$  and  $10^8 \Omega \text{ cm}^2$ . The coating capacitances for all the enamel- and epoxy-coated samples range from  $10^{-10}$  to  $10^{-9} \text{ F/cm}^2$ . The large pore resistance and small coating capacitance indicate that both the enamel and epoxy coatings are strong barriers against the penetration and diffusion of electrolyte. The index  $n_c$  of all the coatings is close to 1, which means that the coatings behave like pure capacitors.

The corrosion rate at the metal surface is inversely proportional to the charge transfer resistance ( $R_{ct}$ ) of the metal sample, which is an indication of how easy electrons can transfer across the metal surface (Ref 26, 27). Among all the samples tested, the uncoated steel samples have the lowest charge transfer resistance of  $381 \pm 42 \Omega \text{ cm}^2$ . The charge transfer resistances of all the coated samples range from  $10^{10}$  to  $10^{11} \Omega \text{ cm}^2$ , which is approximately  $10^8$  times larger than those of the uncoated samples. The double-layer capacitance ( $C_{dl}$ ) is also a measure of the ease of charge transfer across the interface between the substrate steel and electrolyte. The double-layer capacitances of all the coated samples ( $10^{-10}$ - $10^{-9} \text{ F/cm}^2$ ) are approximately  $10^{10}$  times smaller than those ( $7.14 \pm 0.53 \text{ F/cm}^2$ ) of the uncoated samples. The substantially higher charge transfer resistance and lower double-layer capacitance of the enamel- and epoxy-coated samples clearly demonstrate their superior performance in resisting the transfer of electrons across the metal surface.

### 3.4 PP Tests

Potentiodynamic polarization plots of the uncoated, enamel-coated and epoxy-coated samples immersed in 3.5 wt.% NaCl solution are presented in Fig. 6 to illustrate the overall kinetics of the corrosion process. It can be seen from Fig. 6 that the anodic portion of polarization curves for all the samples tested shows the same changing trend although some fluctuations can be observed from the uncoated steel samples. The fluctuations are likely because the existing rusts or corrosion products formed on the surface of uncoated steel samples affect the diffusion of oxygen and water molecule (Ref 28).

The corrosion potential ( $E_{\text{corr}}$ ) and corrosion current density derived from the potentiodynamic polarization plots are presented in Fig. 7a-c. These bar charts show the average plus/minus one standard deviation of each electrochemical parameter from the tests of three identical samples. The corrosion potentials of all the enamel- and epoxy-coated samples are positive with the highest value of 0.88 V for the powder enamel coating while those of the uncoated samples are negative with an average value of  $-0.62 \text{ V}$ . The corrosion potentials of powder and slurry enamel-coated samples as shown in Fig. 7a are consistent with the OCPs as displayed in Fig. 3. The corrosion potentials of the uncoated and epoxy-coated samples are smaller than their OCPs. The uncoated and epoxy-coated samples are thus more susceptible to the disturbance of charging currents than the enamel-coated samples. This is because the changing polarization leads to a continuous variation of the charging current density stored at the substrate-electrolyte interface and the potentiodynamic polarization curve is easily distorted around the corrosion potential where the charging current is hard to be separated directly from the small faradaic current (Ref 29). The average corrosion currents of all the enamel- and epoxy-coated samples are around  $10^{-12} \text{ A}$ ,

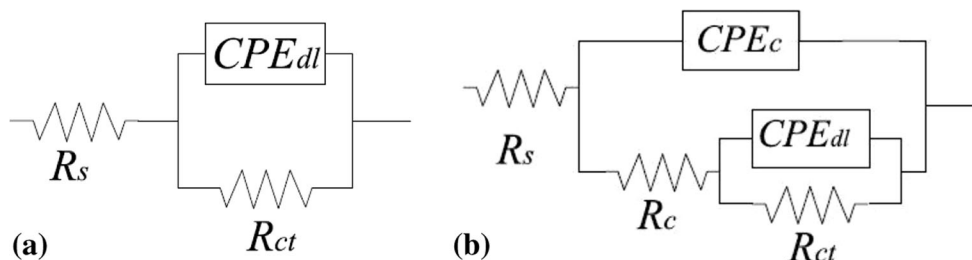
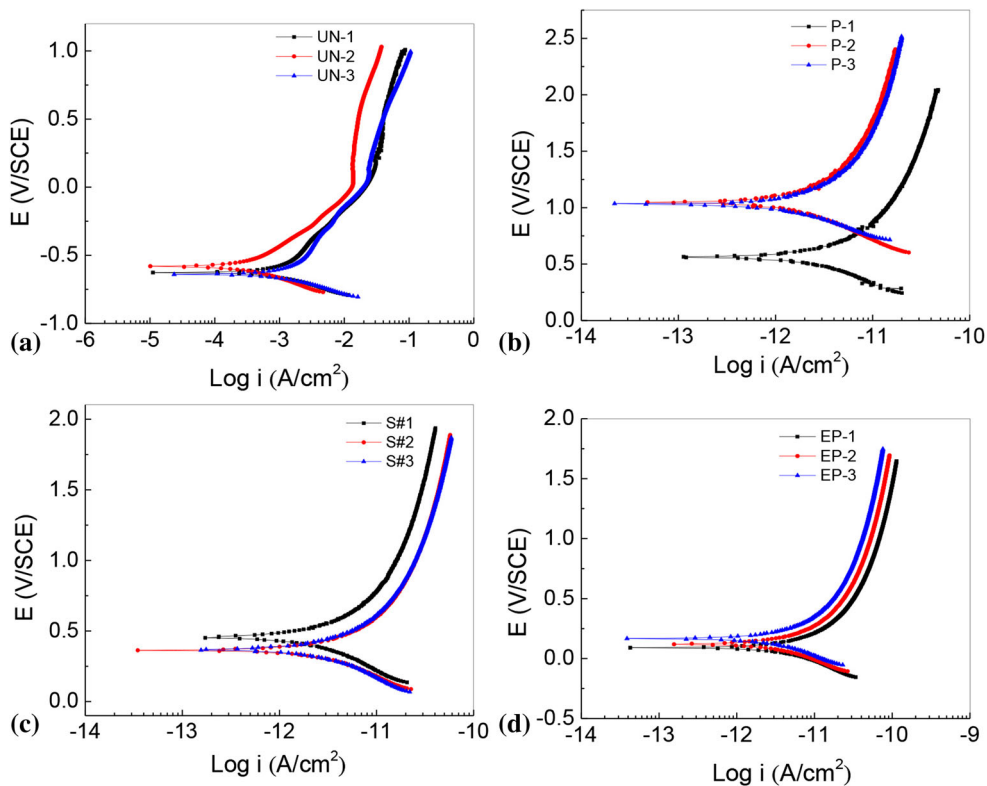


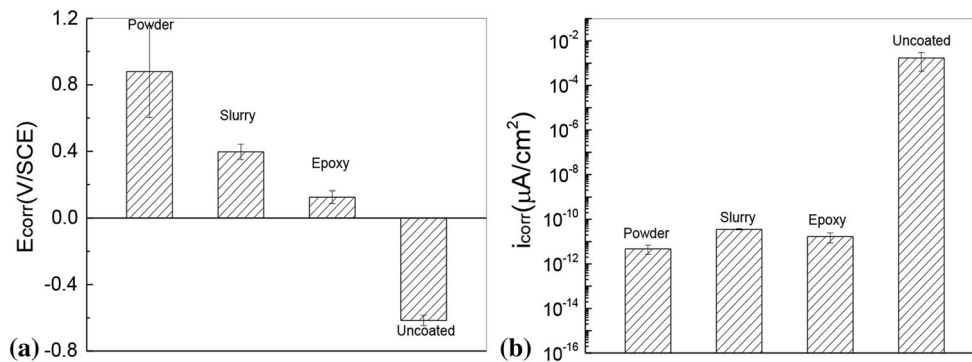
Fig. 5 EEC models for: (a) uncoated, (b) powder enamel-coated, slurry enamel-coated and epoxy-coated samples

Table 2 EEC parameters obtained by fitting into experimental data

	$Y_c, \Omega\text{-sec}^n/\text{cm}^2$	$n_c$	$R_c, \Omega \text{ cm}^2$	$C_c, \text{ F/cm}^2$	$Y_{dl}, \Omega\text{-sec}^n/\text{cm}^2$	$n_{dl}$	$R_{ct}, \Omega \text{ cm}^2$	$C_{dl}, \text{ F/cm}^2$
P-1	$4.26 \times 10^{-10}$	0.98	$2.56 \times 10^7$	$3.96 \times 10^{-10}$	$2.24 \times 10^{-10}$	0.65	$3.22 \times 10^{10}$	$6.57 \times 10^{-10}$
P-2	$3.38 \times 10^{-10}$	0.99	$4.72 \times 10^7$	$3.22 \times 10^{-10}$	$1.38 \times 10^{-10}$	0.63	$4.84 \times 10^{10}$	$4.24 \times 10^{-10}$
P-3	$3.71 \times 10^{-10}$	0.99	$2.71 \times 10^7$	$3.57 \times 10^{-10}$	$1.70 \times 10^{-10}$	0.69	$4.44 \times 10^{10}$	$4.23 \times 10^{-10}$
S-1	$4.58 \times 10^{-10}$	0.99	$4.37 \times 10^7$	$4.36 \times 10^{-10}$	$2.01 \times 10^{-10}$	0.64	$3.99 \times 10^{10}$	$6.43 \times 10^{-10}$
S-2	$4.21 \times 10^{-10}$	0.99	$3.40 \times 10^7$	$4.00 \times 10^{-10}$	$2.06 \times 10^{-10}$	0.63	$2.94 \times 10^{10}$	$5.80 \times 10^{-10}$
S-3	$4.06 \times 10^{-10}$	0.99	$3.54 \times 10^7$	$3.84 \times 10^{-10}$	$1.88 \times 10^{-10}$	0.64	$2.87 \times 10^{10}$	$4.87 \times 10^{-10}$
EP-1	$2.84 \times 10^{-10}$	0.98	$3.42 \times 10^7$	$2.56 \times 10^{-10}$	$3.09 \times 10^{-10}$	0.67	$1.46 \times 10^{10}$	$6.40 \times 10^{-10}$
EP-2	$3.12 \times 10^{-10}$	0.98	$6.39 \times 10^7$	$2.83 \times 10^{-10}$	$3.11 \times 10^{-10}$	0.71	$1.83 \times 10^{10}$	$6.29 \times 10^{-10}$
EP-3	$2.91 \times 10^{-10}$	0.98	$3.78 \times 10^7$	$2.64 \times 10^{-10}$	$2.79 \times 10^{-10}$	0.69	$2.26 \times 10^{10}$	$6.34 \times 10^{-10}$
UN-1	—	—	—	—	0.15	0.52	386	6.54
UN-2	—	—	—	—	0.17	0.53	422	7.31
UN-3	—	—	—	—	0.13	0.49	337	7.56



**Fig. 6** Potentiodynamic polarization curves for: (a) uncoated, (b) powder enamel-coated, (c) slurry enamel-coated and (d) epoxy-coated steel samples



**Fig. 7** Electrochemical parameters extracted from potentiodynamic polarization curves: (a) corrosion potential, (b) corrosion current density

which are about  $10^9$  times smaller than that of the uncoated samples. Thus, all the coatings can protect the substrate metal from corrosion.

during corrosion tests, and the enamel coatings are effective barriers to protect substrate steel from corrosion.

#### 4. Coating Characterization After Corrosion Tests

Cross-sectional SEM images and representative EDS analyses of enamel-coated steel samples after corrosion tests are presented in Fig. 8. Compared with the SEM images and EDS analyses before corrosion tests in Fig. 2, the coating microstructure, bonding interface between the coating and steel and principal components remain basically the same in powder and slurry enamel coatings. The sodium content changes little and chloride is not detected by EDS analyses. Therefore, the electrolyte did not penetrate through the coatings

#### 5. Conclusions

Based on the experimental results and analysis, the following conclusions can be drawn:

1. The thicknesses of powder and slurry enamel coatings are 180 and 235  $\mu\text{m}$ , corresponding to a porosity content of 3.51 and 6.57%, respectively. The powder enamel coating contains fewer but larger isolated air bubbles than the slurry enamel coating. Both coatings cope with small iron protrusions very well, which ensure strong bonding between the coatings and their substrate steel.

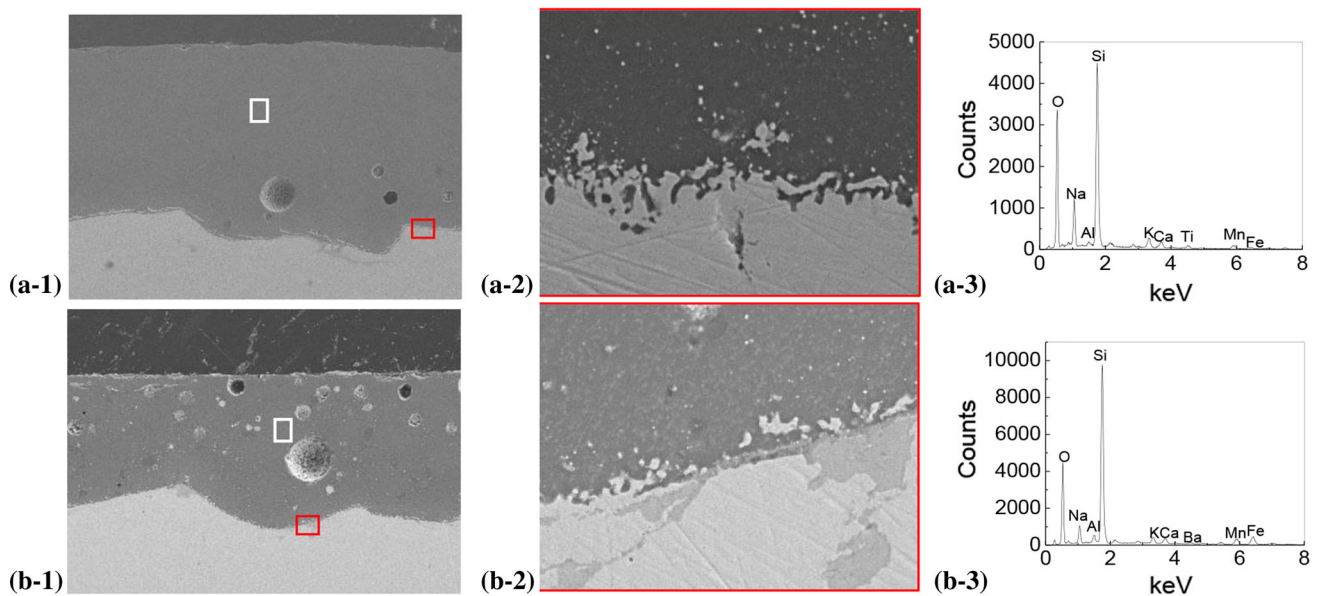


**Fig. 8** Cross-sectional SEM images and EDS analysis of (a-1, a-2, a-3) powder enamel-coated sample and (b-1, b-2, b-3) slurry enamel-coated sample after corrosion tests with different magnifications: (a-1) 250 $\times$ , (a-2) 2500 $\times$ , (b-1) 250 $\times$  and (b-2) 2500 $\times$

- The open-circuit potentials of three uncoated steel samples decreased to an average value of  $-0.48$  V after 1 h of immersion in 3.5 wt.% NaCl solution while those of the enamel- and epoxy-coated samples are positive. This comparison implies that both the enamel and epoxy coatings behave like a barrier for corrosion protection.
- EIS tests showed that the impedances of both enamel- and epoxy-coated samples at a low frequency of 5 mHz were approximately  $10$  G $\Omega$  cm $^2$ , and the phase angles at high frequency approached to  $90^\circ$ . These results demonstrate that these coatings provided excellent corrosion protection for the substrate steel.
- Potentiodynamic polarization tests showed that all the enamel- and epoxy-coated samples had a positive corrosion potential and a significantly lower corrosion rate current than the uncoated samples.
- Comparison of the SEM images and EDS analyses of two enamel-coated steel samples before and after corrosion tests shows nearly the same coating microstructure and the same enamel-steel interface with no presence of chloride. Therefore, the electrolyte did not penetrate through either the powder or slurry enamel coating during corrosion tests, both effectively protecting substrate steel from corrosion.
- The powder enamel coating applied through the electrostatic spray process has a smoother surface and higher corrosion resistance than the slurry enamel coating. In addition, the electrostatic process requires less coating time and is thus a practical solution in pipeline field applications.

### Acknowledgment

The authors gratefully acknowledge the financial support provided by the US Department of Transportation under Award No. DTPH5615HCAP10. The findings and opinions expressed in this paper are those of the authors only and don't necessarily reflect the views of the sponsor.

### References

- PHMSA: Stakeholder Communications—Internal Corrosion. <[https://primis.phmsa.dot.gov/comm/FactSheets/FSInternalCorrosion.htm?no\\_cache=2447](https://primis.phmsa.dot.gov/comm/FactSheets/FSInternalCorrosion.htm?no_cache=2447)>
- NACE International. Managing Corrosion of Pipelines That Transport Crude Oils. Pipeline and Gas Journal, March, 2013, vol. 240, no. 3. <<https://pgjonline.com/2013/03/04/managing-corrosion-of-pipelines-that-transport-crude-oils/>>
- S. Prabhu. Gas Pipelines: Internal Corrosion Protection and Fire Prevention. Corrosionpedia Newsletter. January 1, 2016
- A. Kehr, *Fusion-Bonded Epoxy Internal Linings and External Coatings for Pipeline Corrosion Protection, Piping Handbook*, NACE International, Houston, 2003
- P.A. Schweitzer, *Corrosion-Resistant Piping Systems*, CRC Press, Boca Raton, 1994, p 193
- F. Tang, G. Chen, R.K. Brow, J.S. Volz, and M.L. Koenigstein, Corrosion Resistance and Mechanism of Steel Rebar Coated with Three Types of Enamel, *Corros. Sci.*, 2012, **59**, p 157–168
- S. Rossi, N. Parziani, and C. Zanella, Abrasion Resistance of Vitreous Enamel Coatings in Function of Frit Composition and Particles Presence, *Wear*, 2015, **332**, p 702–709
- A.P. Kozlova, N.I. Guba, and I.A. Drobot, Comparative Testing of One-Coat Enamels for Pipes, *Glass Ceram.*, 2001, **58**(1-2), p 72–74
- O.R. Lazutkina, M.G. Kostenko, S.A. Komarova, and A.K. Kazak, Highly Reliable Energy-Efficient Glass Coatings for Pipes Transporting Energy Carriers, Liquids, and Gases, *Glass Ceram.*, 2007, **64**(3-4), p 93–95
- I.G. Berdenishvili, Synthesis of Low-Melting Pipe Enamel Coatings and Their Chemical Durability, *Am. J. Mater. Sci.*, 2016, **6**(2), p 45–48
- A.V. Ryabova, E.A. Yatsenko, V.V. Khoroshavina, and L.V. Klimova, Glass-Enamel Corrosion-Resistant Coatings for Steel Pipelines, *Glass Ceram.*, 2017, **74**(7-8), p 282–287
- H.H. Liu, Y. Shueh, F.S. Yang, and P. Shen, Microstructure of the Enamel-Steel Interface: Cross-Sectional TEM and Metallographic Studies, *Mater. Sci. Eng. A*, 1992, **149**(2), p 217–224
- X. Yang, A. Jha, R. Brydson, and R.C. Cochrane, An Analysis of the Microstructure and Interfacial Chemistry of Steel-Enamel Interface, *Thin Solid Films*, 2003, **443**(1), p 33–45
- Y. Zuo, R. Pang, W. Li, J.P. Xiong, and Y.M. Tang, The Evaluation of Coating Performance by the Variations of Phase Angles in Middle and High Frequency Domains of EIS, *Corros. Sci.*, 2008, **50**(12), p 3322–3328



15. L. Fan, F. Tang, S.T. Reis, G. Chen, and M.L. Koenigstein, Corrosion Resistance of Transmission Pipeline Steel Coated with Five Types of Enamels, *Acta Metallurgica Sinica (English Letters)*, 2017, **30**, p 390
16. F. Tang, Y. Bao, Y. Chen, Y. Tang, and G. Chen, Impact and Corrosion Resistances of Duplex Epoxy/Enamel Coated Plates, *Constr. Build. Mater.*, 2016, **112**, p 7–18
17. M.R. Presa, R.I. Tucceri, M.I. Florit, and D. Posadas, Constant Phase Element Behavior in the Poly (o-toluidine) Impedance Response, *J. Electroanal. Chem.*, 2001, **502**(1), p 82–90
18. Z. Yao, Z. Jiang, and F. Wang, Study on Corrosion Resistance and Roughness of Micro-Plasma Oxidation Ceramic Coatings on Ti Alloy by EIS Technique, *Electrochim. Acta*, 2007, **52**(13), p 4539–4546
19. M.E. Orazem and B. Tribollet, *Electrochemical Impedance Spectroscopy*, 1st ed., Wiley, Hoboken, 2008, p 233 (ISBN: 978-0-470-04140-6)
20. C. Zhu, R. Xie, J. Xue, and L. Song, Studies of the Impedance Models and Water Transport Behaviors of Cathodically Polarized Coating, *Electrochim. Acta*, 2011, **56**(16), p 5828–5835
21. B. Hirschorn, M.E. Orazem, B. Tribollet, V. Vivier, I. Frateur, and M. Musiani, Determination of Effective Capacitance and Film Thickness from Constant-Phase-Element Parameters, *Electrochim. Acta*, 2010, **55**(21), p 6218–6227
22. P. Córdoba-Torres, T.J. Mesquita, O. Devos, B. Tribollet, V. Roche, and R.P. Nogueira, On the Intrinsic Coupling Between Constant-Phase Element Parameters  $\alpha$  and  $Q$  in Electrochemical Impedance Spectroscopy, *Electrochim. Acta*, 2012, **72**, p 172–178
23. J. Zhang, J. Hu, J. Zhang, and C. Cao, Studies of Water Transport Behavior and Impedance Models of Epoxy-coated Metals in NaCl Solution by EIS, *Prog. Org. Coat.*, 2004, **51**(2), p 145–151
24. G.W. Walter, A Review of Impedance Plot Methods Used for Corrosion Performance Analysis of Painted Metals, *Corros. Sci.*, 1986, **26**(9), p 681–703
25. Y. Zuo, R. Pang, W. Li, J.P. Xiong, and Y.M. Tang, The Evaluation of Coating Performance by the Variations of Phase Angles in Middle and High Frequency Domains of EIS, *Corros. Sci.*, 2008, **50**(12), p 3322–3328
26. F. Tang, X. Cheng, G. Chen, R.K. Brow, J.S. Volz, and M.L. Koenigstein, Electrochemical Behavior of Enamel-Coated Carbon Steel in Simulated Concrete Pore Water Solution with Various Chloride Concentrations, *Electrochim. Acta*, 2013, **92**, p 36–46
27. H.H. Hassan, E. Abdelghani, and M.A. Amin, Inhibition of Mild Steel Corrosion in Hydrochloric Acid Solution by Triazole Derivatives: Part I. Polarization and EIS Studies, *Electrochim. Acta*, 2007, **52**(22), p 6359–6366
28. F. Tang and G. Chen, Chemically Reactive Enamel Coating of Steel Rebar for Enhanced Durability of Reinforced Concrete Structures, *Int. J. Struct. Eng.*, 2015, **6**(1), p 56–72
29. X.L. Zhang, ZhH Jiang, ZhP Yao, Y. Song, and DWu Zh, Effects of Scan Rate on the Potentiodynamic Polarization Curve Obtained to Determine the Tafel Slopes and Corrosion Current Density, *Corros. Sci.*, 2009, **51**(3), p 581–587